ELSEVIER

17 October 1997

Chemical Physics Letters 277 (1997) 521–526

CHEMICAL PHYSICS LETTERS

Thermally induced failure mechanisms of organic light emitting device structures probed by X-ray specular reflectivity

P. Fenter [a,1], F. Schreiber [a], V. Bulović [b,c], S.R. Forrest [b,c]

[a] *Princeton Materials Institute, Princeton University, Princeton, NJ 08544, USA*
[b] *Center for Photonics and Optoelectronic Materials, Princeton University, Princeton, NJ 08544, USA*
[c] *Department of Electrical Engineering, Princeton University, Princeton, NJ 08544, USA*

Received 2 June 1997; in final form 4 August 1997

Abstract

The thermal evolution of organic light emitting device structures and materials has been measured using X-ray specular reflectivity. Thermally induced failure of these structures is found to be due to the large thermal expansion of the hole transport layer (N,N′-diphenyl-N,N′-bis(3-methylphenyl)1,1′-biphenyl-4,4′diamine, or TPD) associated with its low glass transition temperature, suggesting a strain-driven failure mechanism (as opposed to TPD recrystallization). These results suggest the possibility of optimizing organic light emitting devices through direct in-situ measurements of their structure and stability. © 1997 Elsevier Science B.V.

Organic light emitting devices (OLED) represent a new basis for light emissive flat panel displays [1–3]. In their simplest form, efficient OLEDs based on vacuum deposited organic films consist of a layer for electron transport and light emission, and a second layer for hole transport. The OLED luminosity is due to the recombination of excitons near the organic–organic heterointerface [4]. At present, OLED lifetime is one of the primary issues limiting the widespread commercial use of these devices, consequently an understanding of their degradation mechanisms is of broad interest [5].

While many studies have addressed the question of OLED degradation from a macroscopic perspective [2,5–8], little is known about the relationship between the molecular-level structure and the device performance characteristics (e.g., luminosity and lifetime) [2,3]. Nevertheless, it is expected that both the charge injection at the metal–organic contact, and the efficiency of formation and recombination of excitons at the organic–organic interface may depend critically upon interfacial structure.

The green emitting OLED consisting of a heterostructure of tris-(8-hydroxyquinoline)aluminum (Alq_3), and N,N′-diphenyl-N,N′-bis(3-methylphenyl)1,1′-biphenyl-4,4′diamine (TPD), has been widely investigated [4,5,8]. Although the microscopic origin of failure remains unclear, a number of studies [5,7] suggest that failure of these OLEDs may be associated with the thermal degradation of the hole transport layer, TPD, which has a low glass transition temperature [9] ($T_g = 60°C$). For this reason, TPD has recently [10] been replaced in many

[1] Current address: Argonne National Laboratory, ER-203, Argonne IL 60439, USA.

0009-2614/97/$17.00 © 1997 Elsevier Science B.V. All rights reserved.
PII S0009-2614(97)00941-X

OLEDs with higher-T_g materials such as N,N′-diphenyl-N,N′-bis-(1-napthyl)-1,1′-biphenyl-4,4′diamine (α-NPD). Recent work has also focused upon dark spot defect formation in functioning OLEDs [2,5], although it is not yet known whether the dark spots are due to localized joule heating (e.g., at the organic–organic interface) or to some other non-thermal degradation mechanism.

In this work, we use precision X-ray reflectivity measurements to study the structure and thermal degradation mechanisms of films and heterostructures consisting of the archetype OLED materials: TPD and Alq_3. We find that as-grown Alq_3/TPD heterostructures have molecularly flat interfaces and that their thermal degradation is found to result from the large thermal expansion of TPD near T_g, as opposed to re-crystallization [7], suggesting a strain-driven failure mechanism. These results are consistent with energy-dispersive X-ray studies of similar heterostructures [11].

The films were grown on Si wafers by thermal evaporation, under high vacuum ($< 5 \times 10^{-7}$ Torr) at room temperature and a growth rate of 1–3 Å s^{-1}. The native oxide on the Si surface was etched prior to film growth with a 10% HF acid solution in deionized water. The samples were then placed in a dry N_2 environment (~ 1 week), and transferred to an ultra-high vacuum system in which the diffraction measurements were performed. Data were obtained as a function of the substrate temperature. These studies therefore provide insight into the thermally activated failure mechanisms in the absence of atmospheric contaminants.

The X-ray reflectivity measurements were performed at the Exxon X10B beamline at the National Synchrotron Light Source with an X-ray wavelength of $\lambda = 1.129$ Å. The intensity of the specularly reflected X-ray beam is measured as a function of the total scattering angle, 2Θ, or equivalently, the momentum transfer, Q, which are related by $Q = (4\pi/\lambda)\sin(2\Theta/2)$. The resolution of the spectrometer is estimated from the beam divergence of $\Delta(2\Theta) \approx 0.03°$ to correspond to an X-ray coherence length of $\Lambda = 2\pi/\Delta Q_r = 2200$ Å. The sample was mounted on a tantalum base, which was heated with a filament. The sample temperature was inferred from the temperature of the tantalum base and was measured with a thermocouple with an estimated absolute uncertainty of 10°C, but with a relative uncertainty of ±1°C.

In Fig. 1a, we show the specular reflectivity of a series of thin film structures (thin and bold lines are experimental data and theoretical fits, respectively). These include (i) TPD on Si, (ii) Alq_3 on Si, and (iii)

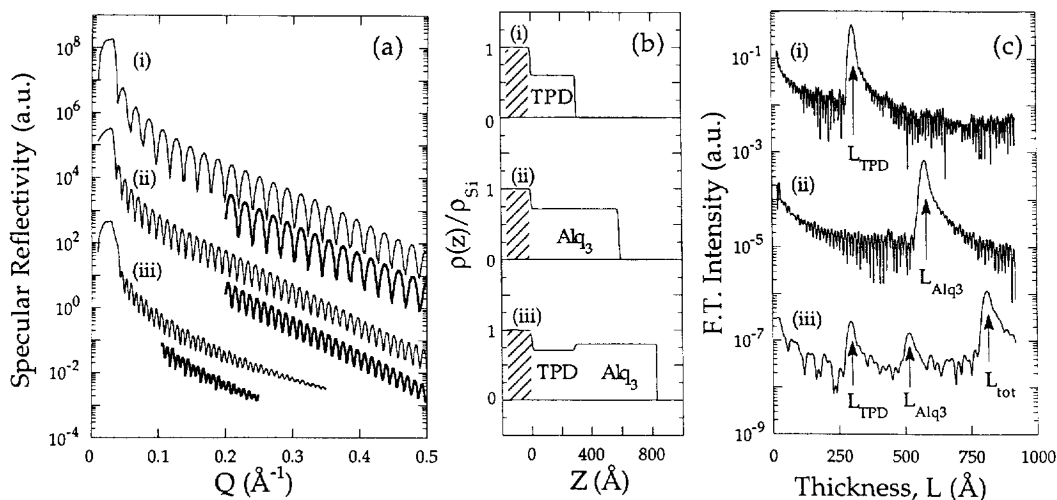

Fig. 1. (a) X-ray specular reflectivity data (thin lines) of (i) Alq_3, (ii) TPD, and (iii) Alq_3/TPD films grown on Si substrates, and corresponding fits (bold lines) using the formalism in Eq. (1). The data and calculations are offset for visual clarity. (b) The electron density profiles derived for each film structure. (c) Fourier transform (FT) of the normalized reflectivity spectra.

Alq_3/TPD on Si, which probe the behavior of the individual OLED materials, as well as the structural interactions between contacting films at the organic–organic interface. The reflectivity spectra are dominated by the Fresnel reflectivity, R_f, of a flat interface [12] which asymptotically follows the form $R_f \approx 1/Q$ [4].

Oscillations in the X-ray reflectivity as a function of the momentum transfer are also clearly observed. The specular reflectivity is related to the laterally averaged electron density profile, $\rho(z)$, through the relations [12]:

$$R(Q) = R_f(Q)|\Phi(Q)|^2, \tag{1a}$$

$$\Phi(Q) = (1/\rho_0)\int(\mathrm{d}\rho/\mathrm{d}z)\,e^{iQz}\,\mathrm{d}z, \tag{1b}$$

where z is the distance from the substrate surface, and ρ_0 is the substrate electron density. That the intensity oscillations in Fig. 1a span a wide range of momentum transfer suggests that the films are very uniform with sharp interfaces. The film structure is determined through a least-squares fit to the data using this formalism (bold lines, Fig. 1a), where we assume a step-wise density profile with Gaussian roughness at each interface [12]. We optimize the fit to the data by minimizing the quality of fit, $S\chi^2 = \Sigma[(R_{calc} - SR_{exp})/\sigma]^2$, where the sum is performed over all data points, R_{calc}, R_{exp}, and σ are the calculated reflectivity, the experimental reflectivity, and the statistical uncertainty for each data point, respectively, and S is an overall scale factor. For convenience, we have not used the data in the small Q regime due to the presence of refraction and multiple scattering. This omission does not affect our results. The analysis reveals the electron density profiles (Fig. 1b) in which all of the interfaces in these three systems are found to have a mean-square roughness of < 4.5 Å. This is comparable to the dimensions of a single molecule, and is $\sim 1\%$ of the total film thickness.

In the case of heterostructures having a step-wise density profile, Eq. (1b) can be converted into a discrete sum over the interfacial density changes, $\Delta\rho_i$. For the case of zero interface roughness,

$$|\Phi(Q)|^2 = \left[\Sigma_i(\Delta\rho_i)^2 + \Sigma_i\Sigma_j\Delta\rho_i\Delta\rho_j\cos(QL_{ij})\right]/(\rho_0)^2, \tag{2}$$

where L_{ij} is the thickness of a layer bounded by interfaces i and j. Eq. (2) suggests that a Fourier transform (FT) of the normalized reflectivity, $R/R_f = |\Phi(Q)|^2$, is a simple method of characterizing the film structure (and is equivalent [12] to a one-dimensional Patterson function of $\mathrm{d}\rho/\mathrm{d}z$). Given the high quality of the reflectivity data, the FT spectra are sensitive to thickness changes of < 1 Å, which we use as the error in our thickness measurements.

In Fig. 1c we show the Fourier transformed normalized reflectivity for each sample derived from data at $Q > 0.04$ Å^{-1}. In the case of the TPD and Alq_3 films, only a single peak is found in each FT spectrum, having a peak intensity which is ~ 2 orders of magnitude above the background, and corresponding to thicknesses of $L_{TPD} = 306$ Å, and $L_{Alq3} = 577$ Å, respectively. In contrast, the Patterson analysis of the Alq_3/TPD heterostructure shows three components, as expected for a two-layer film. These peaks correspond to film thicknesses of $L_{TPD} = 296$ Å, $L_{Alq3} = 518$ Å and $L_{TPD+Alq3} = L_{tot} = 813$ Å.

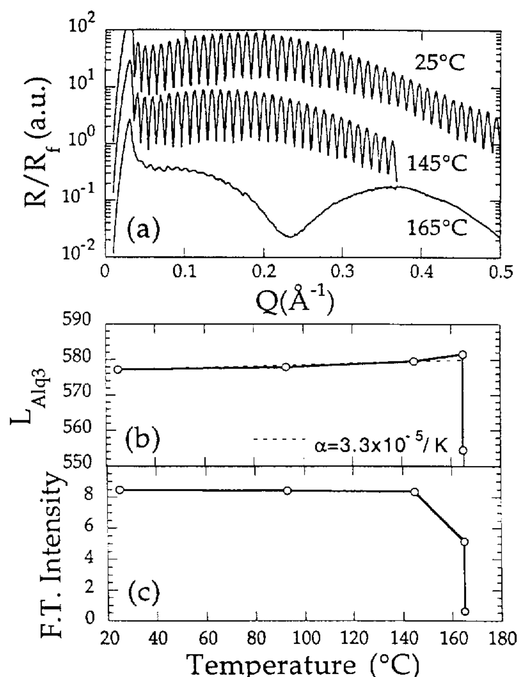

Fig. 2. (a) Normalized specular reflectivity (R/R_f) for Alq_3/Si as a function of substrate temperature. (b) Film thickness, and (c) FT intensity vs. temperature as derived from the FT analysis.

Since Eq. (1) would need to be modified to include the possibility of inhomogeneous structural changes, we explored the thermally induced device failure mechanisms with the model-independent FT analysis. The normalized reflectivity data for Alq_3 on Si (Fig. 2a) clearly show that the film remains unchanged for temperatures as high as 145°C. In Fig. 2b, we plot the temperature dependence of the film thickness and FT intensity obtained from the position and integrated intensity of the peak in the FT spectrum. For $T \leq 145°C$, the only change is due to a small increase in the film thickness corresponding to a thermal expansion coefficient of $\alpha = (3.3 \pm 1) \times 10^{-5}\ K^{-1}$. Above this temperature, the film thickness and FT intensity decrease rapidly and irreversibly. At 165°C, the data reveal that the film is 14 Å thick, which suggests that the changes are due to thermally induced desorption of Alq_3. This provides an upper limit for the useful temperature range of Alq_3.

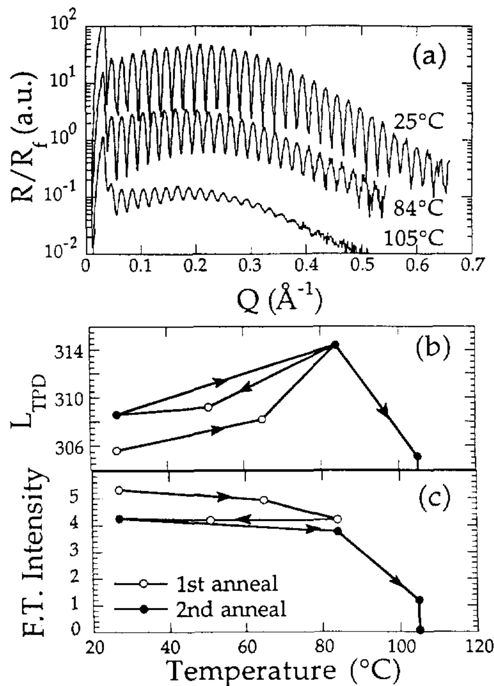

Fig. 3. (a) Normalized specular reflectivity (R/R_f) for TPD/Si vs. substrate temperature. (b) Film thickness, and (c) FT intensity vs. temperature as derived form the FT analysis. The arrows in (b, c) show the thermal history of the sample.

In contrast, TPD/Si (Fig. 3) exhibits a more complex thermal evolution. In the first annealing cycle to 84°C (open circles, Fig. 3b), there is a large (9 Å) increase in film thickness, which nearly reverts to the as-deposited value upon cooling back to room temperature. Since the film becomes 3 Å *thicker* after the first anneal, this suggests that desorption is not important at these temperatures. This change in thickness is also correlated with a small but significant loss in the FT intensity in the first annealing cycle (open circles, Fig. 3c). From these data, we estimate a thermal expansion coefficient for TPD of $\alpha(T < 60°C) = 1.2 \times 10^{-4}\ K^{-1}$, and $\alpha(T > 60°C) \sim 1 \times 10^{-3}\ K^{-1}$. Upon heating to temperatures as high as 105°C during the second annealing cycle (filled circles), we observe a significant decrease in both the film thickness and FT intensity. Subsequent cooling to room temperature shows a decrease in FT intensity of two orders of magnitude, while the nominal film thickness has decreased by only 14%. These data suggest a laterally inhomogeneous desorption process at elevated temperatures, leaving behind small TPD islands whose thickness is nearly unchanged. These data also rule out a simple densification of the TPD layer, as that would result in only a minor change in FT intensity corresponding to a 14% decrease in the film thickness.

An Alq_3/TPD heterostructure on Si was also studied to characterize the thermal response of an OLED. The reflectivity data for the Alq_3/TPD structure (Fig. 4a) show clear but subtle changes in the intensity oscillations at $T \leq 83°C$, providing direct evidence for thermally induced structural changes. We plot the thermal evolution of individual film thicknesses and FT intensities in Fig. 4b and c, respectively. The films exhibit time-dependent structural changes for $T \geq 83°C$ which are characterized by a marked *increase* in L_{TPD} and L_{tot} at 83°C, and which are further enhanced at 90°C. While the FT intensity of all three Fourier components exhibits small ($\sim$ 10%) changes of different signs and magnitude (which may be due to changes in the film structure and/or morphology) at $T = 83°C$, a $\sim$ 50% decrease in the spectral intensity is observed for *all three* Fourier components at $T = 90°C$. After returning the sample to room temperature, no visible film inhomogeneities are observed, suggesting that the behavior is not due to a large-scale macroscopic

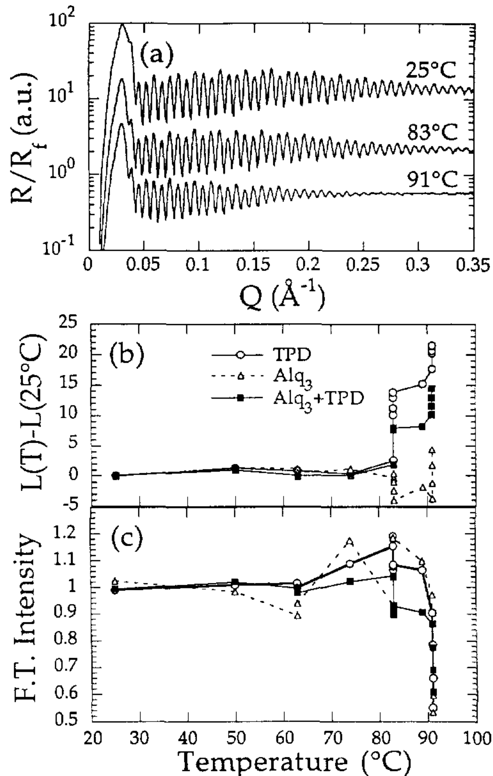

Fig. 4. (a) Normalized specular reflectivity (R/R_f) for Alq_3/TPD/Si vs. substrate temperature. (b) Change in the layer thicknesses, $L_i - L_i(25°C)$ and (c) FT intensity (normalized to 25°C) of each Fourier component is shown.

change in the heterostructure (such as desorption or dewetting).

The thermally induced changes in Fig. 4b and c are not due to roughening of the interfaces, since the integrated FT intensity (as shown in Fig. 4c) is insensitive to interface roughness. In fact, a separate analysis of the data reveals that only a ~50% increase in the roughness of all three interfaces has occurred in this heating process. Furthermore, we can rule out any significant thermal desorption since we observe that *all* three layer thicknesses *increase* with time at the highest temperature studied (90°C). While it has been suggested that the poor thermal stability of TPD is due to recrystallization [7], separate X-ray data (over a wide range of momentum transfer, $0.2\ Å^{-1} \leq Q \leq 2\ Å^{-1}$, under both specular and non-specular conditions) provide no evidence for the formation of microcrystalline TPD or Alq_3 even for the annealed samples. This suggests that recrystallization is not the cause of device failure under our experimental conditions. Note that previous studies [7,11] performed in air also showed no direct evidence for recrystallization, although morphological changes were clearly observed.

The key to understanding the behavior of the Alq_3/TPD heterostructure is found by noting that there is a 5 Å contraction of the Alq_3 layer thickness at 83°C, consistent with the 11 Å increase in the TPD film thickness, and the related 6 Å increase in the total film thickness. The magnitude and sign of the change in L_{Alq3} are both unexpected since an increase in L_{Alq3} of 1.0 Å is expected due to thermal expansion. This suggests that the reduction in Alq_3 layer thickness may be driven by strain build-up in the heterostructure. Here, the thermal expansion of the TPD layer (independently observed in Fig. 3) induces a tensile strain in the Alq_3 layer, thereby reducing the Alq_3 thickness. At 90°C, the large loss of FT intensity of all three thicknesses in the Alq_3/TPD system, and the simultaneous expansion of the Alq_3 beyond its room temperature thickness strongly suggests a strain release in the heterostructure at this temperature through an inhomogeneous process such as blistering. Apparently, the fundamental driving force for the degradation of Alq_3/TPD heterojunctions is the large thermal expansion of TPD associated with its glass transition, and which might be driven by local Joule heating in functioning Alq_3/TPD OLEDs. This conclusion is also consistent with observations that Alq_3/TPD structures grown at elevated temperatures ($T = 73°C$) exhibit greater thermal stability than those grown at room temperature [8].

In conclusion, we have demonstrated the use of X-ray reflectivity for direct in-situ studies of the structural and thermal instabilities of OLEDs. Similar measurements may provide a rapid means of characterizing the behavior of new OLED materials, as well as determining the temporal evolution of OLEDs under stressed operating conditions. More detailed structural studies of the metal–organic and organic–organic interfaces may also help to determine the characteristics which are favorable for charge injection, exciton formation, and recombination at these interfaces.

Acknowledgements

This work was supported by NSF MRSEC award number DMR-94-00362, the AFOSR (M. Prairie), and the Universal Display Corporation. FS acknowledges the support of the DFG (SCHR537/2-1). This work was performed at the NSLS which is supported by DOE Contract No. DE-AC0276CH-00016.

References

[1] C.W. Tang, S.A. VanSlyke, Appl. Phys. Lett. 51 (1987) 913.
[2] J.R. Sheats, H. Antoniadis, M. Hueshen, W. Leonard, J. Miller, R. Moon, D. Roitman, A. Stocking, Science 273 (1996) 884.
[3] L.J. Rothberg, A.J. Lovinger, J. Mater. Res. 11 (1996) 3174.
[4] P.E. Burrows, Z. Shen, V. Bulović, D.M. McCarty, S.R. Forrest, J. Appl. Phys. 79 (1996) 7991.
[5] P.E. Burrows, V. Bulović, S.R. Forrest, L.S. Sapochak, D.M. McCarty, M.E. Thompson, Appl. Phys. Lett. 65 (1994) 2922.
[6] F. Papadimitrakopoulos, X.-M. Zhang, D.L. Thomsen III, K.A. Higginson, Chem. Mater. 8 (1996) 1363.
[7] E. Han, L. Do, Y. Niidome, M. Fujihira, Chem. Lett. (Japan) (1994) 969.
[8] Y. Sato, H. Kanai, Mol. Cryst. Liq. Cryst. 253 (1994) 143.
[9] K. Naito, A. Miura, J. Phys. Chem. 97 (1993) 6240.
[10] S.A. VanSlyke, C.H. Chen, C.W. Tang, Appl. Phys. Lett. 69 (1996) 2160.
[11] K. Orita, T. Morimura, T. Horiuchi, K. Matsuchige, Int. Conf. on Electrolum. of Molec. Mat. and Related Phenom., Kitakuishu, Japan, May, 1997, Pap. 23-0-08.
[12] I.M. Tidswell, B.M. Ocko, P.S. Pershan, S.R. Wasserman, G.M. Whitesides, J.D. Axe, Phys. Rev. B 41 (1990) 1111.